Journal of Alloys and Compounds 872 (2021) 159743

Contents lists available at ScienceDirect

Journal of Alloys and Compounds

journal homepage: www.elsevier.com/locate/jalcom

Microstructure and thermoelectric properties of the medium-entropy block-textured $BiSbTe_{1.5}Se_{1.5}$ alloy

Oleg Ivanov[a,*], Maxim Yaprintsev[b], Alexei Vasil'ev[a], Ekaterina Yaprintseva[a,b]

[a] Belgorod State Technological University named after V.G. Shukhov, Belgorod 308012, Russian Federation
[b] Belgorod State University, Belgorod 308015, Russian Federation

ARTICLE INFO

Article history:
Received 15 January 2021
Received in revised form 24 March 2021
Accepted 27 March 2021
Available online 2 April 2021

Keywords:
High-entropy and medium entropy alloys
Thermoelectric materials
Lattice thermal conductivity
Spark plasma sintering
Texturing
Block-textured structure

ABSTRACT

Medium-entropy $BiSbTe_{1.5}Se_{1.5}$ alloy has been prepared by self-propagating high-temperature synthesis (to prepare a starting powder with desired composition and structure) and spark plasma sintering (to prepare block-textured samples). Under texturing, a partial ordering of grains, which is typical for Bi_2Te_3-based alloys, takes place resulting in forming a lamellar grain structure. Lamellar sheets are not continuous for whole volume of the textured sample. There are blocks with continuous lamellar sheets of some definite orientation, but the orientations of the sheets in neighboring blocks are different from each other. Forming the block-textured structure can be related to specific features of the starting powder, applied to sinter the bulk samples. The starting powder was strongly inhomogeneous and particles in the starting powder were rather big and shape-isotropic. As result, the texturing can be initiated in local domains of volume independently from each other resulting in forming the blocks with different preferential grains orientation. Due to the block texturing, the thermoelectric properties of the $BiSbTe_{1.5}Se_{1.5}$ alloy, measured perpendicularly or parallel to a texturing axis, are different. Many features, found in these properties, are typical for textured Bi_2Te_3-based alloys. The thermoelectric properties of the medium-entropy block-textured $BiSbTe_{1.5}Se_{1.5}$ alloy can be believed to be promising enough. The highest thermoelectric figure-of-merit equal to ~0.43 was observed for the perpendicular measuring orientation. This alloy can be next applied as a precursor for developing five- or six-element high-entropy alloys with enhanced thermoelectric efficiency.

1. Introduction

Developing high-entropy alloys is one of fruitful and effective approaches of modern materials science that can be applied to improve the properties of both structural and functional materials [1–5]. The high-entropy alloys consist of five or more principal elements in equimolar or near-equimolar ratios, which compete for the same position in a crystal lattice. Due to effects of the high-mixing entropy and chemical complexity, the high-entropy alloys show many unique properties, useful for variety of applications. Besides the high-entropy alloys, medium-entropy alloys consisting of 3 or 4 principal elements are also intensively developed and examined [6–8]. Generally, the medium-entropy alloys should be considered as precursors, which can be applied to prepare the high-entropy alloys by adding other principal elements. The medium-entropy alloys have simpler structure, composition and, hence, properties, which can be taken as reference ones for the relevant high-entropy alloys.

Owing to effective scattering of phonons by lattice disorder, which is formed in the high-entropy and medium-entropy alloys, these alloys possess intrinsically low lattice thermal conductivity. This feature is very important to enhance the thermoelectric efficiency of materials [9–13]. Actually, the thermoelectric figure-of-merit, ZT, is expressed as $ZT = [PF/k_t]T$, where T is the absolute temperature, k_t is the total thermal conductivity with contributions from the lattice thermal conductivity, k_p, the electronic thermal conductivity, k_e, the bipolar thermal conductivity, k_b, (this contribution is specific for semiconductors) and PF is the power factor [14]. In turn, PF is given as $PF = S^2/\rho$, where ρ is the specific electrical resistivity and S is the Seebeck coefficient. Therefore, due to the low lattice thermal conductivity, the high-entropy and medium-entropy alloys can be considered as a new class of promising thermoelectric materials. At present, direct way to develop these materials is based on applying known thermoelectric compound taken as some starting material, which can be transformed into the high-entropy and medium-entropy alloy. In accordance with this approach,

* Corresponding author.
E-mail address: Ivanov.Oleg@bsu.edu.ru (O. Ivanov).

https://doi.org/10.1016/j.jallcom.2021.159743
0925-8388/

bismuth telluride, Bi_2Te_3, was successfully applied as the starting material to develop both high-entropy $(BiSbTe_{1.5}Se_{1.5})_{1-x}Ag_x$ and medium-entropy $BiSbTe_{1.5}Se_{1.5}$ alloys [15,16]. The bismuth telluride itself is widely applied to prepare *n*-$Bi_2Te_{3-x}Se_x$ and *p*-$Bi_{2-x}Sb_xTe_3$ alloys for low-temperature thermoelectric applications [17,18]. It is known that the Bi_2Te_3-based alloys are readily texturing under uniaxial pressuring [19–25]. Moreover, the texturing is one of key parameters affecting the thermoelectric properties of these materials, since it results in a partial recovering of natural crystal anisotropy in the properties inherent to single-crystalline Bi_2Te_3 [26]. Therefore, the texturing effect on the thermoelectric properties of the high-entropy and medium-entropy alloys, derived from Bi_2Te_3 structure, should be also taken into account to characterize the properties in detail.

The main aim of this paper is to examine features in the microstructure and thermoelectric properties of the medium-entropy textured $BiSbTe_{1.5}Se_{1.5}$ alloy. Self-propagating high-temperature synthesis (SHS) was used to prepare a starting powder. In contrast to common methods of chemical synthesis, the SHS-process is very fast. By now, it was successfully applied to prepare a wide range of the thermoelectric materials [27–30]. To texture the alloy being studied, spark plasma sintering (SPS) was applied. The SPS method is often applied to prepare various Bi_2Te_3-based materials with improved and governed thermoelectric properties [19,20,22,31,32].

2. Materials and methods

To prepare the starting powder, Bi, Sb, Se and Te powders taken in a stoichiometric ratio were thoroughly mixed. Then the mixture was cold-pressed into pellets under uniaxial 50 MPa pressure. The pellets were put in a quartz ampule. To start the SHS-process, a bottom of the ampule was heated by a hand torch under continuous evacuating by a pump. Once ignited, the hand torch was immediately removed. The SHS-process was finishing in several seconds. After finishing the SHS-process, the synthesized sinter was grounded for 30 min, resulting in the starting $BiSbTe_{1.5}Se_{1.5}$ powder. To prepare bulk samples, the starting powder was spark-plasma-sintered at pressure of 40 MPa and temperature of 723 K for 15 min in vacuum. Density of the bulk samples was measured by the Archimedes' method. X-ray diffraction (XRD) analysis of the starting powder and bulk samples was performed by using a Rigaku Ultima IV diffractometer with CuK_α-radiation. Scanning electron microscopy (SEM, a Nova NanoSEM 450 microscope) was applied to examine morphology of the starting powder and grain structure of the bulk samples. To measure the thermoelectric properties of the bulk samples, the 2 × 2 × 10 mm bars and the Ø10 × 2 mm disks were prepared. A ZEM-3 system was applied for the ρ and S measuring of the bar samples. A TC-1200 system was applied for the k_t measuring by using the disk-shaped samples.

3. Results and discussion

XRD pattern for the starting powder taken at room temperature is presented in Fig. 1. According to XRD analysis, the powder is single hexagonal phase with space symmetry $R\bar{3}m$ group (PDF#01-089-4302). This crystal structure is characteristic for pure Bi_2Te_3 and Bi_2Te_3-based alloys. Unit cell parameters, which were calculated by the Rietveld refinement, are $a = b = 4.179$ Å and $c = 28.701$ Å. According to SEM examination, the powder consists of various size particles having mainly irregular shape (Fig. 1(d)). To estimate an average particle size, l_a, a histogram of grain size distribution was plotted. The histogram was fitted by a lognormal unimodal distribution that can be expressed as [33].

$$F(l) = \frac{1}{\sqrt{2\pi}\sigma l}\exp\left(-\frac{(\ln l - \ln l_a)^2}{2\sigma^2}\right), \quad (1)$$

where $F(l)$ is the lognormal probability density function, σ is the standard deviation of logarithms of the particle sizes.

The l_a value was estimated as ~1.55 μm.

The density of the bulk samples was equal to ~6.87 g cm^{-3}. This value is in agreement with data reported in Refs. [15,16]. The bulk samples happened to be textured. The texturing in the Bi_2Te_3-based alloys is usually developing during sintering under uniaxial pressuring of a starting powder consisting of particles with specific shape and size. Generally, the texturing can be confirmed by XRD and SEM examination [26]. Ideally, for highly-textured Bi_2Te_3-based samples with textured structure, which is continuous and homogeneous within whole volume, the intensities of (00 l) peaks should be enhancing for the perpendicular surface, whereas the intensities of (11l) peaks should be increasing for the parallel surface [26]. The continuous and homogeneous textured Bi_2Te_3 structure is readily formed for the starting powder consisting from nm-thin 2D-plateled particles [26]. During the SPS-process, these plates are ordered, and under further high-temperature forming a grain structure, lamellar sheets with preferential grains orientation are arranged. XRD patterns for the perpendicular and parallel surfaces of the samples being studied are presented in Fig. 1(b) and (c). A slight increase in intensity of (00l) peaks can be really observed for the perpendicular surface, however any change in intensity of (11l) peaks for the parallel surface happens to too small to be reliably analyzed. Therefore, the redistribution in intensities of the (00l) and (11l) peaks, which is usually due to the texturing, is minor. However, SEM images of the grain structures, taken for the perpendicular (Fig. 1(e)) and parallel (Fig. 1(f)) surfaces, are rather different. In contrast to the starting powder particles, the grains have a crystal faceting that can be taken as evidence of intense sintering of the powder during the SPS-process. The grains themselves are plate-like shaped, and larger faces of the plates are irregularly shaped. Forming the plate-like grains is typical for the grained Bi_2Te_3-based alloys, and it can by usually attributed to specific features in crystal structure and chemical bonding of Bi_2Te_3 [17,18]. The crystal Bi_2Te_3 structure is layered one. Crystal *c*-axes are oriented perpendicularly to the layers, and crystal *a*-*b* planes are oriented along the layers. Neighboring layers are bonded via weak Van-der-Waals interaction, whereas chemical bonding within the layers is dominantly strong covalent. A rate of grains growth during high-temperature sintering of the grained Bi_2Te_3-based material happens to be rather different for directions, parallel and perpendicular to the layers that results in forming the plate-like grains [26].

Similarly to the grained Bi_2Te_3-based material, under the grain ordering in the $BiSbTe_{1.5}Se_{1.5}$ alloy during the SPS-process, the plate-like grains are arranging in such manner that their flat surfaces are dominantly oriented perpendicularly to the uniaxial SPS pressuring direction (Fig. 1(e)), i.e. crystal *c*-axes of the grains preferentially directed parallel to this direction (Fig. 1(f)). In turn, crystal *a*-*b* planes of the grains are preferentially oriented perpendicularly to the SPS-pressing direction. However, the lamellar sheets, which are formed in textured $BiSbSe_{1.5}Te_{1.5}$ alloy, are not continuous for whole volume. There are blocks with the continuous lamellar sheets of some definite orientation, but the orientations of the sheets in neighboring blocks are different from each other. A size of the blocks is a few dozens of micrometers. Two blocks are highlighted by ellipses in Fig. 1(f). Semi-major axes of the ellipses correspond to the dominant grains orientation in the blocks I and II. In contrast to nm-thin 2D-plateled particles, applied to prepare highly-textured Bi_2Te_3-based samples with continuous and homogeneous textured structure, the particles in the starting $BiSbTe_{1.5}Se_{1.5}$ powder consisted of micron size particles having mainly irregular shape (Fig. 1(d)). That is this starting powder is, firstly, strongly inhomogeneous, secondly, the particles in the starting powder are rather big and shape-isotropic. In this case, the texturing can be initiated in local domains of volume independently from each other, resulting in forming the

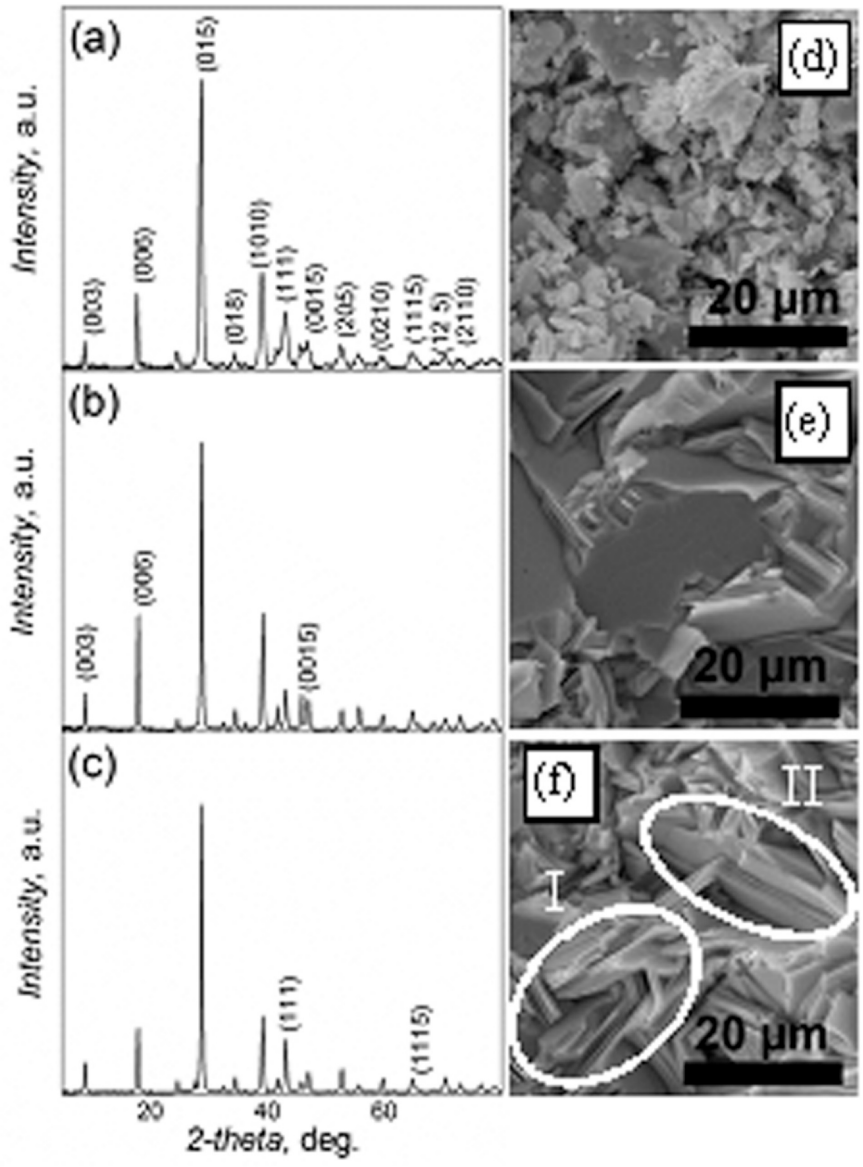

Fig. 1. XRD patterns (left panel) and SEM images (right panel) for the starting powder ((a) and (d)) and the bulk sample taken for the fractured surfaces, oriented perpendicularly ((b) and (e)) and parallel ((c) and (f)) to the SPS-pressuring direction.

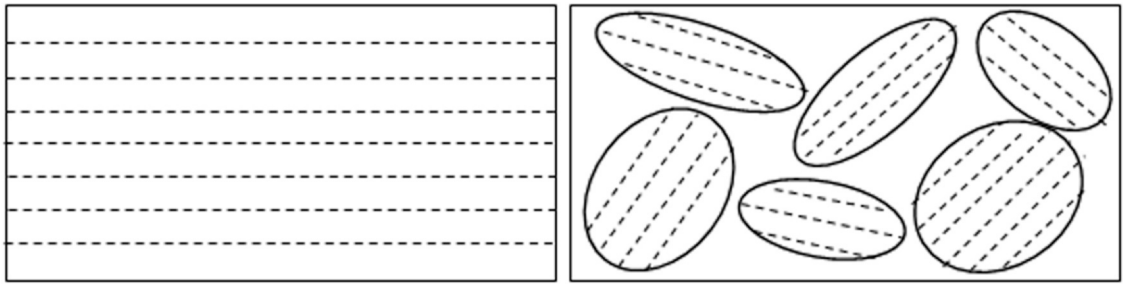

Fig. 2. Schematic illustrations of ideally textured (left) and block-textured (right) samples (lamellar sheets with preferential grains orientations correspond to dashed lines).

block-textured structure. Schematic illustrations of ideally textured and block-textured (right) samples are shown in Fig. 2.

To estimate average values of lateral size, D_a, and thickness, d_a, of the grains in the blocks, relevant histograms of lateral size and thickness distributions were plotted, which were again analyzed in framework of the lognormal unimodal distribution. The D_a and d_a values were estimated as ~12.0 and ~4.2 μm, respectively. Hence, the samples being studied are micro-grained ones. A grain shape factor, D_a/d_a, introduced to characterize a difference in the grain sizes, is equal to 2.86, i.e. really the grains are rather shape-anisotropic.

To estimate a texturing degree for the samples being studied, the Lotgering factor, *LF*, was extracted via analysis of XRD pattern, taken for the perpendicular surface. *LF* is known to given by expression [34].

$$F = \frac{p - p_0}{1 - p_0} \quad (2)$$

where p and p_0 are defined as

$$p = \frac{I(00l)}{\sum I(hkl)}, \text{ and } p_0 = \frac{I_0(00l)}{\sum I_0(hkl)}, \quad (3)$$

and the I_0 and I intensities correspond to non-textured (non-oriented) and textured (oriented) samples, respectively.

LF happened to be equal to ~0.13. That is the samples being studied are weakly block-textured.

Since the $BiSbTe_{1.5}Se_{1.5}$ alloy is texturing under the SPS process, its thermoelectric properties are anisotropic. To find the texturing effect, the thermoelectric properties were measured for directions, perpendicular (perpendicular measuring orientation, $\rho_\perp$, $k_\perp$ and $S_\perp$) and parallel (parallel measuring orientation, ρ_{II}, k_{II} and S_{II}) to the SPS-pressing direction. The texturing results in redistribution of anisotropic ρ and k contributions from crystal *a*-*b* plane (ρ_{ab} and k_{tab}) and *c*-axis (ρ_c and k_{tc}) into the specific electrical resistivity and the total thermal conductivity, which are measured parallel or perpendicularly to the texturing axis [26]. At the parallel measuring orientation, ρ_c and k_{tc} are dominant contributions, whereas at the perpendicular measuring orientation the electrical and thermal properties are determined by ρ_{ab} and k_{tab}. Since $\rho_{ab} < \rho_c$ and $k_{ab} > k_c$, the electrical resistivity increases and the thermal conductivity decreases for the parallel measuring orientation as compared to these properties for the perpendicular measuring orientation. For the Bi_2Te_3-based alloys, the Seebeck coefficient is weakly anisotropic quantity [26]. Similar features with minor differences were also found in the thermoelectric properties of the block-textured $BiSbTe_{1.5}Se_{1.5}$ alloy.

The $\rho(T)$ dependences of the samples being studied are presented in Fig. 3(a). Within whole temperature range under study, ρ for the parallel measuring orientation (curve *1*) is higher as compared to that for the perpendicular measuring orientation (curve *2*). At room temperature, anisotropy coefficient of the specific electrical resistivity can be estimated as $\rho_{II}/\rho_\perp \approx 1.28$, i.e. the texturing effect on ρ is rather remarkable. For both measuring orientations, ρ is gradually growing with increasing temperature. This $\rho(T)$ behavior is usually observed in metals and degenerate semiconductors. It is known that the specific electrical resistivity of donor semiconductors is given as [35].

$$\rho = \frac{1}{e\mu n}, \quad (4)$$

where e, n and μ are the unit charge, concentration and mobility of electrons, respectively.

Generally, the $\rho(T)$ behavior can be dependent on both $n(T)$ and $\mu(T)$ changes. The degenerate semiconductors, n is T-independent, i.e. the $\rho(T)$ changes in Fig. 3(a) are related to the $\mu(T)$ changes.

Similarly to the Bi_2Te_3-based alloys, the Seebeck coefficient in the block-textured $BiSbTe_{1.5}Se_{1.5}$ alloy is also weakly anisotropic quantity ($S_\perp/S_{II} \approx 1$), since the $S(T)$ curves, taken for the perpendicular and parallel measuring orientations, are positioned very close to each other (Fig. 3(b)). Since a sign of S is negative, majority carriers in the samples being studied are electrons. The Seebeck coefficient of degenerate donor semiconductor is expressed as [36].

$$S = \frac{2k_B^2 T m^*}{3e\hbar^2}\left(\frac{\pi}{3n}\right)^{2/3}\left(\frac{3}{2} + \gamma\right), \quad (5)$$

where k_B is the Boltzmann's constant, $\hbar$ is the reduced Planck constant, m^* is the density-of-state effective mass of electrons, and γ is the scattering factor.

According to expression (5), S should be linearly increasing with increasing temperature. As is shown by dashed lines in Fig. 3(b), T-linear growth of S is really observed within a broad temperature range. However, maxima in the $S(T)$ dependences are observed at

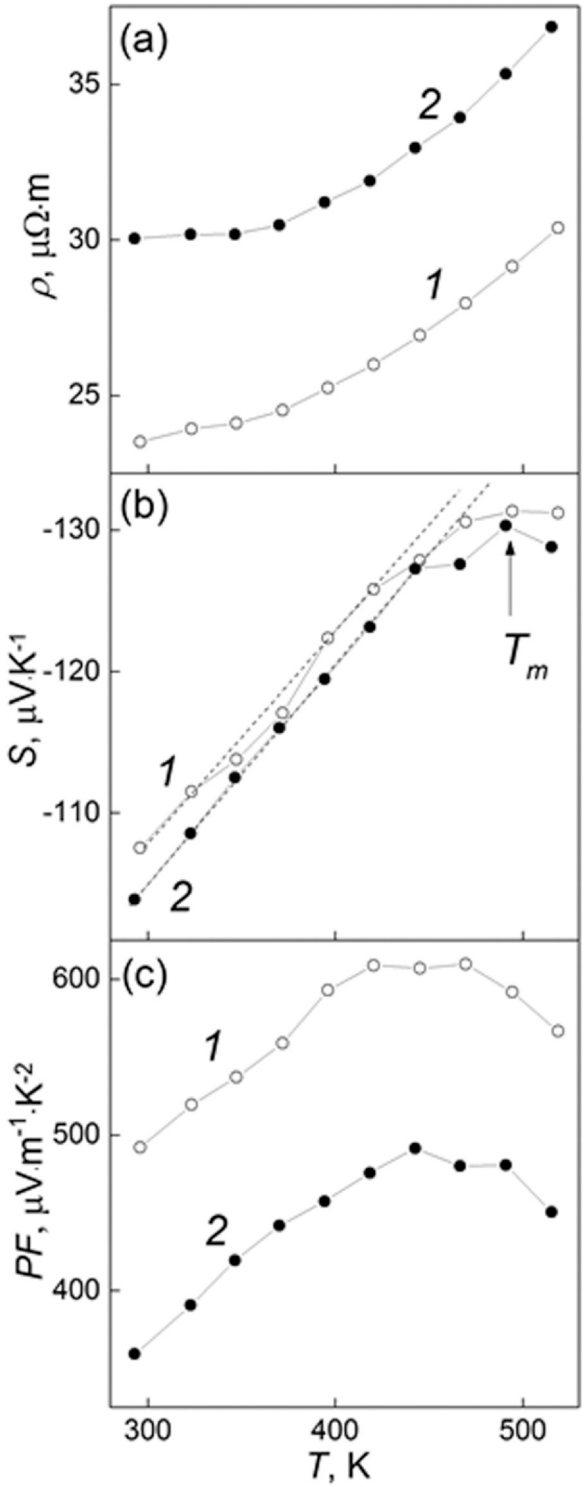

Fig. 3. The temperature dependences of ρ (a), S (b) and PW (c) for bulk sample, taken for the perpendicular (curves *1*) and parallel (*2*) measuring orientations.

$T_m \approx 490$ K. These maxima are originated from a bipolar effect, which is characteristic for the Bi_2Te_3-based alloys [37–41]. In contrast to the Bi_2Te_3-based alloys, onset of intrinsic conductivity resulting in the bipolar effect is not clearly observed in the $\rho(T)$ behavior (Fig. 3(a)).

By using the Goldsmid-Sharp expression, the $S(T)$ dependences were applied to estimate a band gap, E_g, in the samples being studied. According to this expression, E_g, maximum value of the Seebeck coefficient ($|S|_{max}$) and temperature at which it takes place (T_{max}), are related by expression [42].

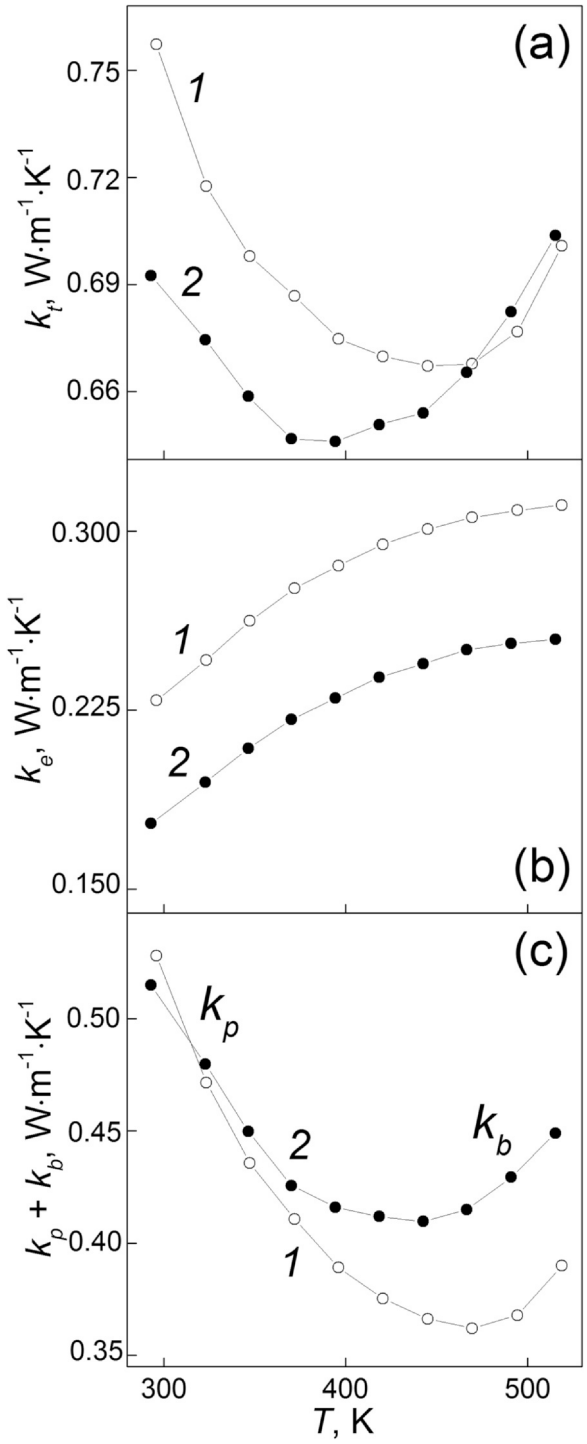

Fig. 4. The temperature dependences of the k_t (a), k_e (b) and $k_p + k_b$ (c) contributions for bulk sample, taken for the perpendicular (curves *1*) and parallel (*2*) measuring orientations.

$$E_g = 2e\ |S|_{max} T_{max} \tag{6}$$

E_g was estimated as ~0.13 eV. This estimate is in well accordance with the E_g value, which is known for Bi_2Te_3 [17].

The $PF(T)$ dependence are presented in Fig. 3(c). Owing to difference of the ρ and S contributions, dependent on the measuring orientation, PF for the perpendicular orientation is less as compared to that for the parallel orientation.

The $k_t(T)$ dependences are presented in Fig. 4(a). Below ~450 K, the thermal conductivity is higher for the perpendicular measuring orientation (curve *1*) as compared to that for the parallel measuring orientation (curve *2*). At room temperature, anisotropy coefficient of the total thermal conductivity was estimated as $k_{t\perp}/kt_{\parallel} \approx 1.09$. So, the texturing effect on k_t is less expressed as compared to that for the texturing effect on ρ. The difference in $k_{t\perp}/kt_{\parallel}$ and $\rho_{\parallel}/\rho_{\perp}$, observed in the block-textured $BiSbTe_{1.5}Se_{1.5}$ alloy, is in agreement in anisotropy of the thermoelectric properties of the Bi_2Te_3-based alloys [26]. At high temperatures, the $k_t(T)$ curves taken for both measuring orientations lie very close to each other. Besides, both $k_t(T)$ curves have minima. The minima are typical for the Bi_2Te_3-based alloys. The lattice thermal conductivity, k_p, the electronic thermal conductivity, k_e, and the bipolar thermal conductivity, k_b, are usually contributing into the total thermal conductivity of semiconductors. The electronic thermal conductivity is related to the specific electrical conductivity, $\sigma = 1/\rho$, by the Wiedemann–Franz law [43].

$$k_e = L\sigma T, \tag{7}$$

where L is a constant called as the Lorenz number.

Approach proposed in Ref. [44] was applied to estimate the Lorenz number for semiconductors. According to the approach, L and maximum S value are linked as

$$L\,[10^{-8}, \mathrm{W{\cdot}\Omega{\cdot}K^{-2}}] = 1.5 + \exp\left(-\frac{|S|_{max}\,[\mu\mathrm{V{\cdot}K^{-1}}]}{116}\right) \tag{8}$$

By using expression (8), for the sample being studied, L was estimated as ~1.8×10^{-8} WΩ K^{-2}. This L value was applied to find the $k_e(T)$ contributions into k_t, as shown in Fig. 4(b). Naturally, the $k_e(T)$ contributions are correlated with the $\rho(T)$ dependences presented in Fig. 3(a), i.e. k_e for the perpendicular measuring orientation (curve *1*) is higher as compared to that for the parallel measuring orientation (curve *2*), and anisotropy coefficient of the electron thermal conductivity is $k_{e\perp}/k_{e\parallel} \approx 1.28$.

The sums of the lattice and bipolar thermal conductivity contributions to the total thermal conductivity were next extracted as $k_p(T) + k_b(T) = k_t(T) - k_e(T)$ (Fig. 4(c)). Similarly to the $k_t(T)$ curves, these contributions have minima, too. The minima are originated from a change in mechanism of the thermal conductivity. For temperatures below the minima, the thermal conductivity is governed by the lattice thermal conductivity, since the summarized $k_p(T) + k_b(T)$ contributions to the total thermal conductivity is gradually decreasing with increasing temperature. Above the Debye temperature, the lattice thermal conductivity is decreasing with increasing temperature obeying a T^{-1} law [35]. For these temperatures, the phonon specific heat is T-independent (in accordance with the Dulong–Petit law). Phonon energy and number of phonons is linearly increasing with increasing temperature. Scattering rate is proportional to the number of phonons, hence, k_p will be also decreasing with increasing temperature. This mechanism can be responsible for the $k_p(T) + k_b(T)$ behavior below the k_p minima. The lattice thermal conductivity happened to be very low (~0.36 for the perpendicular measuring orientation at ~475 K). As was mentioned above, the low lattice thermal conductivity is specific feature of the high-entropy and medium-entropy alloys, which are characterized by structural and compositional disorder.

Above the minima in the $k_p(T) + k_b(T)$ curves, these summarized contributions already increase with increasing temperature. This growth should be attributed to the bipolar thermal conductivity. Due to the intrinsic conductivity, electron-hole pairs start to be thermally excited at hot-side of sample. Then, these pairs move to cold-side, where they are recombined, and energy of recombination per one pair is equal or greater than the band gap. This energy is emerged as a phonon, which transfers a heat. The bipolar thermal conductivity can be expressed as [45].

$$k_b = \frac{\sigma_n \cdot \sigma_p}{\sigma_n + \sigma_p}(S_p - S_n)^2 T, \tag{9}$$

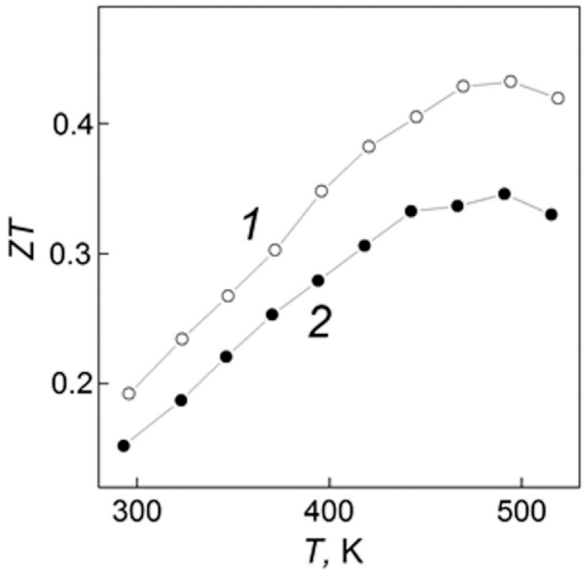

Fig. 5. The temperature dependences of *ZT* for bulk sample, taken for the perpendicular (curves *1*) and parallel (*2*) measuring orientations.

where σ_i and S_i (subscript $i = n, p$) are the partial electrical conductivity and Seebeck coefficient for electrons and holes, respectively. In turn, σ_i of each carrier is $\sigma_i = ie\mu_i$ where $i = n, p$ designates the electron and hole concentration, respectively.

It should be noted that the lattice thermal conductivity happens to be isotropic within the temperature range studied, since the $k_p(T)$ dependences, taken for both measuring orientations, are positioned very close to each other, whereas the bipolar thermal conductivity is weakly anisotropic, since k_b taken for the perpendicular measuring orientation, is lower as compared to that for the parallel measuring orientation. Therefore, the anisotropy in the total thermal conductivity, which is developing under the texturing, are originated from anisotropy in the electron thermal conductivity and anisotropy in the bipolar thermal conductivity. In accordance with expression (9), the bipolar thermal conductivity is dependent on both the partial electrical conductivities of electrons and holes and the Seebeck coefficients for electrons and holes. As it follows from Fig. 4(b), under the texturing, the electrical resistivity becomes anisotropic that can result in weak anisotropy in the bipolar thermal conductivity. Moreover, a combination of these properties results in lower bipolar thermal conductivity for the perpendicular measuring orientation as compared to that for the parallel measuring orientation. At present, more correct analysis of the texturing effect on the thermal properties of the block-textured $BiSbTe_{1.5}Se_{1.5}$ alloy is rather complicated task. Detailed examination of the samples with various texturing degree should be carried out.

The ρ, S and k values were applied to plot the $ZT(T)$ dependences (Fig. 5). As was discussed above, at texturing, ρ decreases and k_t increases for the perpendicular measuring orientation as compared to these properties for the parallel measuring orientation, and S is independent on the measuring orientation. Since the ρ decrease is stronger than the k_t increase, ZT for the perpendicular measuring orientation is remarkably enhanced. As was mentioned in Introduction part, the thermoelectric performance of the high-entropy and medium entropy alloys are dominantly originated from their low lattice thermal conductivity. The lowest value of the lattice thermal conductivity, $k_{p\ min}$, and the highest value of the thermoelectric figure-of-merit, ZT_{max}, observed for the $BiSbTe_{1.5}Se_{1.5}$ alloy in present work and also reported in Refs. [15,16], are collected in Table 1. The texturing effect on the thermoelectric properties has not been discussed in Refs. [15,16]. Besides, Ag-doping effect on the thermoelectric properties of the $BiSbTe_{1.5}Se_{1.5}$ alloy was found in Ref. [16]. The $(BiSbTe_{1.5}Se_{1.5})_{99.1}Ag_{0.9}$ composition demonstrated the highest ZT_{max} and lowest $k_{p\ min}$ values. The ZT_{max} and $k_{p\ min}$ values presented in Table allow really considering the $BiSbTe_{1.5}Se_{1.5}$ alloy as a precursor thermoelectric material with promising properties. Some difference in the ZT_{max} and $k_{p\ min}$ values can be related to different methods of preparation of the samples studied, their texturing degree, grains size, features in defect structure, etc. It should be noted that the $BiSbTe_{1.5}Se_{1.5}$ alloy being developed in this work is weakly textured. By involving the texturing with higher degree of the grain ordering, the thermoelectric properties of the alloy can be additionally tuned to maximize the thermoelectric figure-of-merit.

4. Conclusion

Thus, the medium-entropy block-textured $BiSbTe_{1.5}Se_{1.5}$ alloy has been prepared by self-propagating high-temperature synthesis and spark plasma sintering. The texturing axis coincides with the SPS pressuring direction. Under the texturing, the lamellar grains structure is formed. The lamellar sheets are not continuous for whole volume of the textured sample. There are blocks with continuous lamellar sheets of some definite orientation, but the orientations of the sheets in neighboring blocks are different from each other. The texturing results in developing of anisotropy in the specific electrical conductivity and thermal conductivity, which are measured perpendicularly and parallel to the texturing axis. Owing to its low lattice thermal conductivity, the thermoelectric performance of the alloy happened to be promising enough. Next step should be transition from the four-element medium-entropy $BiSbTe_{1.5}Se_{1.5}$ alloy to a five- or six-element high entropy alloy based on the precursor $BiSbTe_{1.5}Se_{1.5}$ system. Taking into account similar characteristics of Se and sulfur, S, the five-component high-entropy BiSbTeSeS can be reasonably chosen for further examination.

CRediT authorship contribution statement

Oleg Ivanov: Project administration, Conceptualization. **Maxim Yaprintsev:** Writing - review & editing. **Alexei Vasil'ev:** Investigation. **Ekaterina Yaprintseva**: Investigation.

Declaration of Competing Interest

The authors declare that they have no known competing financial interests or personal relationships that could have appeared to influence the work reported in this paper.

Table 1
The lattice thermal conductivity and thermoelectric figure-of-merit of the medium-entropy $BiSbTe_{1.5}Se_{1.5}$ alloys.

Reference	Composition	$k_{p\ min}$, $W \cdot m^{-1} \cdot K^{-1}$	ZT_{max}
[15]	$BiSbTe_{1.5}Se_{1.5}$	~0.17 at 523 K	~0.43 at 523 K
[16]	$BiSbTe_{1.5}Se_{1.5}$	~0.47 at 425 K	~0.20 at 450 K
[16]	$(BiSbTe_{1.5}Se_{1.5})_{99.1}Ag_{0.9}$	~0.29 at 425 K	~0.63 at 450 K
Present work	$BiSbTe_{1.5}Se_{1.5}$: perpendicularly to texturing axis	~0.36 at 475 K	~0.43 at 450 K
Present work	$BiSbTe_{1.5}Se_{1.5}$: parallel to texturing axis	~0.41 at 440 K	~0.34 at 450 K

Acknowledgments

This work was supported by Ministry of Science and Higher Education of the Russian Federation (grant number No 0625-2020-0015). All of studies were carried out by the scientific equipment of joint research centre "Technologies and Materials" at the Belgorod State University.

References

[1] E.P. George, D. Raabe, R.O. Ritchie, High-entropy alloys, Nat. Rev. Mater. 4 (2019) 515–534, https://doi.org/10.1038/s41578-019-0121-4
[2] Y.F. Ye, Q. Wang, J. Lu, C.T. Liu, Y. Yang, High-entropy alloy: challenges and prospects, Mater. Today 19 (2016) 349–362, https://doi.org/10.1016/j.mattod.2015.11.026
[3] E.P. George, W.A. Curtin, C.C. Tasan, High entropy alloys: a focused review of mechanical properties and deformation mechanisms, Acta Mater. 188 (2020) 435–474, https://doi.org/10.1016/j.actamat.2019.12.015
[4] H.-J. Qiu, G. Fang, Y. Wen, P. Liu, G. Xie, X. Liu, S. Sun, Nanoporous high-entropy alloys for highly stable and efficient catalysts, J. Mater. Chem. A. 7 (2019) 6499–6506, https://doi.org/10.1039/c9ta00505f
[5] L. Sun, R.J. Cava, High-entropy alloy superconductors: Status, opportunities, and challenges, Phys. Rev. Mater. 3 (2019), https://doi.org/10.1103/PhysRevMaterials.3.090301
[6] H. Gasan, M. Zamani, A novel medium entropy alloy based on ironmanganese-aluminum-nickel: influence of boron addition on phase formation, microstructure, and mechanical properties, Mater. Res. Express 7 (2020), https://doi.org/10.1088//2053-1591/ab600f
[7] J.W. Bae, H.S. Kim, Towards ferrous medium-entropy alloys with low-cost and high-performance, Scr. Mater. 186 (2020) 169–173, https://doi.org/10.1016/j.scriptamat.2020.05.030
[8] Y. Zhou, D. Zhou, X. Jin, X. Du, B. Li, Design of non-equiatomic medium-entropy alloys, Sci. Rep. 8 (2018), https://doi.org/10.1038/s41598-018-19449-0
[9] S. Shafeie, S. Guo, Q. Hu, H. Fahlquist, P. Erhart, A. Palmqvist, High-entropy alloys as high-temperature thermoelectric materials, J. Appl. Phys. 118 (2015) 184905, https://doi.org/10.1063/1.4935489
[10] R.-Z. Zhang, F. Gucci, H. Zhu, K. Chen, M.J. Reece, Data-driven design of ecofriendly thermoelectric high-entropy sulfides, Inorg. Chem. 57 (2018) 13027–13033, https://doi.org/10.1021/acs.inorgchem.8b02379
[11] A. Karati, M. Nagini, S. Ghosh, R. Shabadi, K.G. Pradeep, R.C. Mallik, B.S. Murty, U.V. Varadaraju, $Ti_2NiCoSnSb$ – a new half-Heusler type high-entropy alloy showing simultaneous increase in Seebeck coefficient and electrical conductivity for thermoelectric applications, Sci. Rep. 9 (2019) 5331, https://doi.org/10.1038/s41598-019-41818-6
[12] K. Han, H. Jiang, T. Huang, M. Wei, Thermoelectric properties of $CoCrFeNiNb_x$ eutectic high entropy alloys, Crystals 10 (2020), https://doi.org/10.3390/cryst10090762
[13] P.-C. Wei, C.-N. Liao, H.-J. Wu, D. Yang, J. He, G.V. Biesold-McGee, S. Liang, W.-T. Yen, X. Tang, J.-W. Yeh, Z. Lin, J.-H. He, Thermodynamic routes to ultralow thermal conductivity and high thermoelectric performance, Adv. Mater. 32 (2020) 1906457, https://doi.org/10.1002/adma.201906457
[14] G.J. Snyder, Figure of merit ZT of a thermoelectric device defined from materials properties, Energy Environ. Sci. 10 (2017) 2280–2283, https://doi.org/10.1039/c7ee02007d
[15] A. Raphel, P. Vivekanandhan, S. Kumaran, High entropy phenomena induced low thermal conductivity in $BiSbTe_{1.5}Se_{1.5}$ thermoelectric alloy through mechanical alloying and spark plasma sintering, Mater. Lett. 269 (2020) 127672, https://doi.org/10.1016/j.matlet.2020.127672
[16] Z. Fan, H. Wang, Y. Wu, X.J. Liu, Z.P. Lu, Thermoelectric high-entropy alloys with low lattice thermal conductivity, RSC Adv. 6 (2016) 52164–52170, https://doi.org/10.1039/c5ra28088e
[17] H.J. Goldsmid, Bismuth telluride and its alloys as materials for thermoelectric generation, Mater 7 (2014) 2577–2592, https://doi.org/10.3390/ma7042577
[18] H. Scherrer, S. Scherrer, Thermoelectrics Handbook: Macro to Nano, CRC Taylor and Francis, Boca Raton, 2012.
[19] S.D. Bhame, D. Pravarthana, W. Prellier, J.G. Noudem, Enhanced thermoelectric performance in spark plasma textured bulkn-type $BiTe_{2.7}Se_{0.3}$ and p-type $Bi_{0.5}Sb_{1.5}Te_3$, Appl. Phys. Lett. 102 (2013) 211901, https://doi.org/10.1063/1.4807771
[20] A. Vasil'ev, M. Yaprintsev, O. Ivanov, E. Danshina, Anisotropic thermoelectric properties of $Bi_{1.9}Lu_{0.1}Te_{2.7}Se_{0.3}$ textured via spark plasma sintering, Sol. State Sci. 84 (2018) 28–43, https://doi.org/10.1016/j.solidstatesciences.2018.08.004
[21] Y. Morisaki, H. Araki, H. Kitagawa, M. Orihashi, K. Hasezaki, K. Kimura, Bi_2Te_3-related thermoelectric samples with aligned-texture prepared by plastic deformation, Mater. Trans. 46 (2005) 2518–2524, https://doi.org/10.2320/matertrans.46.2518
[22] M. Yaprintsev, A. Vasil'ev, O. Ivanov, Thermoelectric properties of the textured $Bi_{1.9}Gd_{0.1}Te_3$ compounds spark-plasma-sintered at various temperatures, J. Eur. Ceram. Soc. 40 (2020) 742–750 https://doi.org10.1016/j.jeurceramsoc.2018.12.041.
[23] O. Ben-Yehuda, R. Shuker, Y. Gelbstein, Z. Dashevsky, M.P. Dariel, Highly textured Bi_2Te_3-based materials for thermoelectric energy conversion, J. Appl. Phys. 101 (2007) 113707, https://doi.org/10.1063/1.2743816
[24] J.J. Shen, L.P. Hu, T.J. Zhu, X.B. Zhao, The texture related anisotropy of thermoelectric properties in bismuth telluride based polycrystalline alloys, Appl. Phys. Lett. 99 (2011) 124102, https://doi.org/10.1063/1.3643051
[25] X. Yan, B. Poudel, W.S. Liu, G. Joshi, H. Wang, Y. Lan, D. Wang, G. Chen, Z.F. Ren, Experimental studied on anisotropic thermoelectric properties and structures of *n*-type $Bi_2Te_{2.7}Se_{0.3}$, Nano Lett. 10 (2010) 3373–3378, https://doi.org/10.1021/nl101156v
[26] O. Ivanov, M. Yaprintsev, A. Vasil'ev, Comparative analysis of the thermoelectric properties of the non-textured and textured $Bi_{1.9}Gd_{0.1}Te_3$ compounds, J. Solid State Chem. 290 (2020) 121559121559-1-10. https://doi:10.1016/j.jssc.2020.121559.
[27] R. Liu, X. Tan, G. Ren, Y. Liu, Z. Zhou, C. Liu, Y. Lin, C. Nan, Enhanced thermoelectric performance of Te-doped Bi_2Se_{3-x} bulks by self-propagating high-temperatures synthesis, Cryst 7 (2017) 257-1-8. https://doi:10.3390/cryst7090257.
[28] X. Su, F. Fu, Y. Yan, G. Zheng, T. Liang, Q. Zhang, X. Cheng, D. Yang, H. Chi, X. Tang, Q. Zhang, C. Uher, Self-propagating high-temperature synthesis for compound thermoelectrics and new criterion for combustion processing, Nat. Commun. 5 (2014), https://doi.org/10.1038/ncomms5908
[29] G.K. Ren, J.L. Lan, S. Butt, K.J. Ventura, Y.H. Lin, C.W. Nan, Enhanced thermoelectric properties in Pb-doped BiCuSeO oxyselenides prepared by ultrafast synthesis, RSC Adv. 5 (2015) 69878–69885, https://doi.org/10.1039/C5RA13191J
[30] D.W. Yang, X.L. Su, Y.G. Yan, T.Z. Hu, H.Y. Xie, J. He, C. Uher, M.G. Kanatzidis, X.F. Tang, Manipulating the combustion wave during self-propagating synthesis for high thermoelectric performance of layered oxychalcogenide $Bi_{1-x}Pb_xCuSeO$, Chem. Mater. 28 (2016) 4628–4640, https://doi.org/10.1021/acs.chemmater.6b01291
[31] G. Yang, L. Sang, F.F. Yun, D.R.G. Mitchell, G. Casillas, N. Ye, K. See, J. Pei, X. Wang, J.-F. Li, G.J. Snyder, X. Wang, Significant enhancement of thermoelectric figure of merit in BiSbTe-based composites by incorporating carbon microfiber, Adv. Funct. Mater. (2021) 2008851, https://doi.org/10.1002/adfm.202008851
[32] G. Yang, R. Niu, L. Sang, X. Liao, D.R.G. Mitchell, N. Ye, J. Pei, J.-F. Li, X. Wang, Ultra-high thermoelectric performance in bulk BiSbTe/amorphous boron composites with nano-defect architectures, Adv. Energy Mater. 10 (2021), https://doi.org/10.1002/aenm.202000757
[33] F.J. Humphreys, M. Hatherly, Recrystallization and Related Annealing Phenomena, Elsevier, Oxford, UK, 2004.
[34] F.K. Lotgering, Topotactical reactions with ferrimagnetic oxides having hexagonal crystal structures—I, J. Inorg. Nucl. Chem. 9 (1959) 113–123, https://doi.org/10.1016/0022-1902(59)80070-1
[35] J.S. Blakemore, Solid State Physics, Cambridge University Press, Cambridge, 1985.
[36] K.C. Lukas, W.C. Liu, Z.F. Ren, C.P. Opeil, Transport properties of Ni, Co, Fe, Mn doped $Cu_{0.01}Bi_2Te_{2.7}Se_{0.3}$ for thermoelectric device applications, J. Appl. Phys. 112 (2012) 054509, https://doi.org/10.1063/1.4749806
[37] O. Ivanov, M. Yaprintsev, R. Lyubushkin, O. Soklakova, Enhancement of thermoelectric efficiency in Bi_2Te_3 via rare earth element doping, Scr. Mater. 146 (2018) 91–94, https://doi.org/10.1016/j.scriptamat.2017.11.031
[38] M. Yaprintsev, R. Lyubushkin, O. Soklakova, O. Ivanov, Effects of Lu and Tm doping on thermoelectric properties of Bi_2Te_3, J. Electron. Mater. 47 (2018) 1362–1370, https://doi.org/10.1007/s11664-017-5940-8
[39] O. Ivanov, M. Yaprintsev, Mechanisms of thermoelectric efficiency enhancement in Lu-doped Bi_2Te_3, Mater. Res. Express 5 (2018) 015905, https://doi.org/10.1088/2053-1591/aaa265
[40] W.Y. Shi, F. Wu, K.L. Wang, J.J. Yang, H.Z. Song, X.J. Hu, Preparation and thermoelectric properties of yttrium-doped Bi_2Te_3 flower-like nanopowders, J. Electron. Mater. 43 (2014) 3162–3168, https://doi.org/10.1007/s11664-014-3220-4
[41] J. Yang, F. Wu, Z. Zhu, L. Yao, H. Song, X. Hu, Thermoelectrical properties of lutetium-doped Bi_2Te_3 bulk samples prepared from flower-like nanopowders, J. Alloy. Compd. 619 (2015) 401–405, https://doi.org/10.1016/j.jallcom.2014.09.024
[42] H.J. Goldsmid, J.W. Sharp, Estimation of the thermal band gap of a semiconductor from Seebeck measurements, J. Electron. Mater. 28 (1999) 869–872, https://doi.org/10.1007/s11664-999-0211-y
[43] W. Liu, X. Yan, G. Chen, Z. Ren, Recent advances in thermoelectric nanocomposites, Nano Energy 1 (2012) 42–56, https://doi.org/10.1021/acs.jpcc.0c01311
[44] H. Kim, Z. Gibbs, Y. Tang, H. Wang, G. Snyder, Characterization of Lorenz number with Seebeck coefficient measurement, APL Mater. 3 (2015) 041506, https://doi.org/10.1063/1.4908244
[45] S. Wang, J. Yang, T. Toll, J. Yang, W. Zhang, X. Tang, Conductivity-limiting bipolar thermal conductivity in semiconductors, Sci. Rep. 5 (2015), https://doi.org/10.1038/srep10136